Journal of ELECTRONIC MATERIALS, Vol. 47, No. 8, 2018
https://doi.org/10.1007/s11664-018-6366-7
© 2018 The Minerals, Metals & Materials Society

Analysis and Modeling of Fullerene Single Electron Transistor Based on Quantum Dot Arrays at Room Temperature

VAHIDEH KHADEM HOSSEINI,[1,2,5] MOHAMMAD TAGHI AHMADI,[2,3,4] and RAZALI ISMAIL[4]

1.—Institute of Nanoscience and Nanotechnology, University of Kashan, Kashan, Iran. 2.—Department of Electrical Engineering, Pardis of Urmia University, Urmia, Iran. 3.—Nanotechnology Research Center, Nano Electronic Research Group, Physics Department, Urmia University, Urmia, Iran. 4.—Faculty of Electrical Engineering, Universiti Teknologi Malaysia, 81310 UTM Johor Bahru, Johor, Malaysia. 5.—e-mail: vahideh_khademhosseini@yahoo.com

The single electron transistor (SET) as a fast electronic device is a candidate for future nanoscale circuits because of its low energy consumption, small size and simplified circuit. It consists of source and drain electrodes with a quantum dot (QD) located between them. Moreover, it operates based on the Coulomb blockade (CB) effect. It occurs when the charging energy is greater than the thermal energy. Consequently, this condition limits SET operation at cryogenic temperatures. Hence, using QD arrays can overcome this temperature limitation in SET which can therefore work at room temperature but QD arrays increase the threshold voltage with is an undesirable effect. In this research, fullerene as a zero-dimensional material with unique properties such as quantum capacitance and high critical temperature has been selected for the material of the QDs. Moreover, the current of a fullerene QD array SET has been modeled and its threshold voltage is also compared with a silicon QD array SET. The results show that the threshold voltage of fullerene SET is lower than the silicon one. Furthermore, the comparison study shows that homogeneous linear QD arrays have a lower CB range and better operation than a ring QD array SET. Moreover, the effect of the number of QDs in a QD array SET is investigated. The result confirms that the number of QDs can directly affect the CB range. Moreover, the desired current can be achieved by controlling the applied gate voltage and island diameters in a QD array SET.

Key words: Coulomb blockade, fullerene, nanoscale, quantum dot arrays, single electron transistor, threshold voltage

INTRODUCTION

Moore's law predicted that the number of transistors in each chip doubles every 2 years, so a CMOS transistor size should be smaller.[1] On the other hand, its scaling below 10 nm has limitations such as leakage current and leakage power.[2–4] Hence, these limitations can be solved by a single electron transistor (SET). This single electron device operates based on the Coulomb blockade (CB) effect. Moreover, this electronic device works by electron tunneling from source to the quantum dot (QD) and then this electron transfers to drain, as shown in Fig. 1.[5–13]

SET has two categories based on the number of QDs: the single dot SET and the multi-dot SET. An electron passes through two tunnel junctions in the first type, while in the second type one electron tunnels to a dominant conducting path called a multi-tunnel junction SET.[14,15] Furthermore, a QD array SET has a higher critical temperature than a single dot SET because the capacitances of

(Received January 9, 2018; accepted May 5, 2018; published online May 21, 2018)

additional dots are in series. Therefore, its effective capacitance reduces and, consequently, this reduction increases the threshold voltage. Hence choosing fullerene as a zero-dimensional material with amazing properties such as quantum capacitance and high critical temperature can overcome this undesirable effect with a consequent increase in the reliability of a QD array SET.[16] The structure of a fullerene SET based on QD arrays is shown in Fig. 2.

BASIC EQUATIONS SET

The SET contains a QD that is located between two tunnel junctions. They consist of a capacitance and a resistance, therefore electrons transfer from capacitors C_1 or C_2 and then the current moves in the SET circuit, as shown in Fig. 3.[10,11,17]

The rate of single electron tunneling is a key factor. Furthermore, it is determined based on an energy balance equation in electron tunneling. The tunneling rate on the right side, r, and the tunneling rate on the left side, l, are given by[18–20]

$$r(n,V) = \frac{1}{e^2 R_1} \frac{E_\mathrm{r} - E_\mathrm{m}}{1 - \mathrm{e}^{-(E_\mathrm{r} - E_\mathrm{m})/k_\mathrm{B}T}} \quad (1)$$

$$l(n,V) = \frac{1}{e^2 R_2} \frac{E_\mathrm{r} - E_\mathrm{m}}{1 - \mathrm{e}^{-(E_\mathrm{r} - E_\mathrm{m})/k_\mathrm{B}T}} \quad (2)$$

where e is the charge of an electron, R_1 the resistance of the tunnel junction, T the temperature, K_B the Boltzmann constant, E_r the Fermi energy of the right electrode and E_m the Fermi energy of the island. $E_\mathrm{r} - E_\mathrm{m}$ is the energy of an electron during the tunneling event as follows:

$$E_\mathrm{r} - E_\mathrm{m} = -\frac{(2n+1)e^2}{2(C_1 + C_2)} + \frac{eC_2 v}{C_1 + C_2} \quad (3)$$

where n is the number of electrons, e the charge of an electron, v the applied gate voltage, and C_1 and C_2 are capacitances of the tunnel junctions.

The probability of tunneling rate $\rho(V, n, t)$ can be given by

$$\begin{aligned}(\partial\rho(V,n,t))/\partial t &= [r_i(n-1,V) + l_i(n-1,V)]\rho(n-1,V,t) \\ &+ [l_i(n+1,V) + r_i(n+1,V)]\rho(n+1,V,t) \\ &- [r_i(n,V) + r_i(n,V) + l_i(n,V)]\rho(n,V,t)\end{aligned} \quad (4)$$

where r_i is the tunneling rate of the right side and l_i the tunneling rate of the left side to QD, n the number of electrons in time t and v the applied gate voltage.

Finally, the current of SET can be calculated by[21]

$$\begin{aligned} I &= \sum_{N=-\infty}^{+\infty} e[r_2(n,V) - l_2(n,V)]\rho(n,V) \\ &= \sum_{N=-\infty}^{+\infty} e[r_1(n,V) - l_2(n,V)]\rho(n,V) \end{aligned} \quad (5)$$

where e is the charge of an electron, r, l are the tunneling rates from the right and left sides, respectively, the $\rho(n, v)$ is the probability of electron transfer.

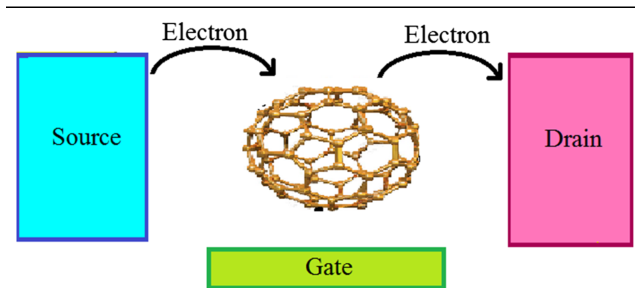

Fig. 1. The electron tunneling in SET.

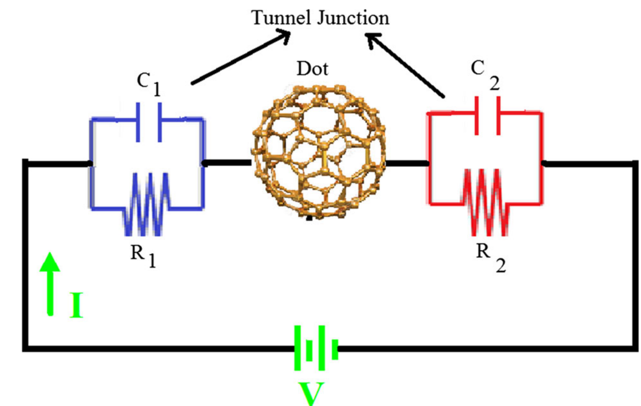

Fig. 3. A single dot SET system.

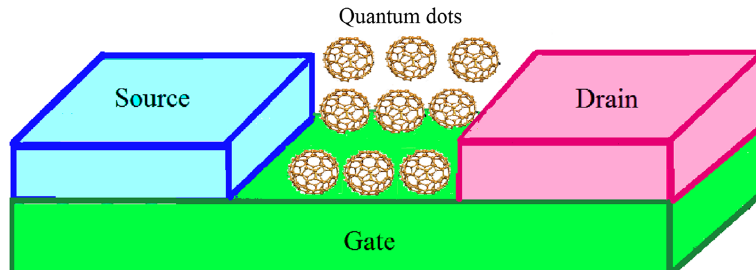

Fig. 2. The structure of a fullerene SET based on QD arrays.

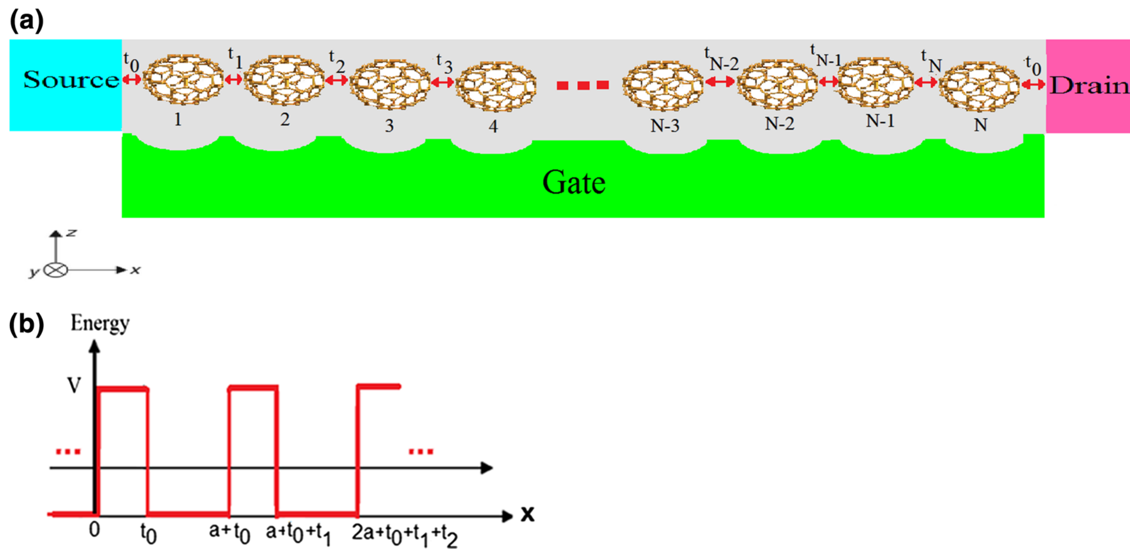

Fig. 4. (a) Schematic of a SET with homogeneous linear QD arrays. (b) SET energy versus channel regions which indicates tunnel barriers.

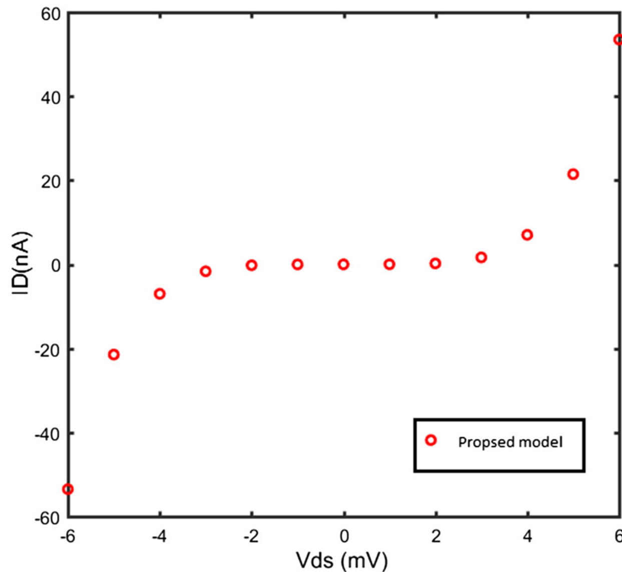

Fig. 5. I–V curve of a homogenous linear QD array fullerene SET at room temperature.

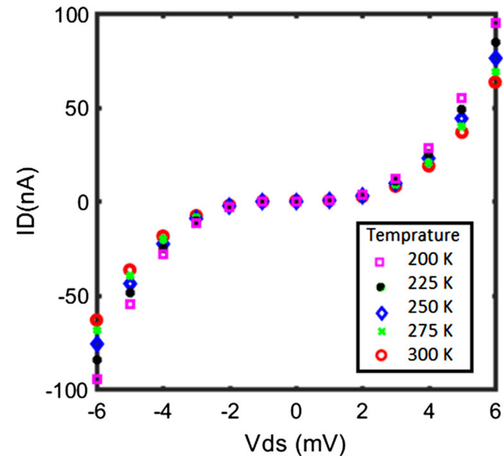

Fig. 6. I–V curves of a homogenous linear QD array fullerene SET at different temperatures.

CURRENT MODEL ON SET WITH FULLERENE QD ARRAYS

The SETs can switch electron tunneling to achieve an amplified current by quantum mechanical effects. Furthermore, the wave crosses several regions, so different wave functions can be written. SET is divided into parts which involve QDs and tunnel junctions. In the following, the drain current of the SET based on two-state QD arrays as homogeneous linear arrays and ring arrays are investigated. There is a cooperative effect between the dots but this small effect is neglected in the present model of fullerene QD arrays.[22,23] The homogeneous linear arrays are shown in Fig. 4a. The energy as a function of SET channel length by considering some barriers is depicted in Fig. 4b and then its regions are expressed by Schrödinger's equations.

The Schrödinger's equations of fullerene SET parts with attention to their areas are written in the following. Each of the QDs is assumed a potential well. The distance between QDs are equal together as $t_0 = t_1 = t_2 = \cdots = t_n$.

$$\frac{-\hbar^2}{2m}\frac{\mathrm{d}^2\psi_{n-1}(x)}{\mathrm{d}x^2} = E\psi_{n-1}(x) \quad n = 2, 4, 6, \ldots, N \tag{6}$$

$$\frac{-\hbar^2}{2m}\frac{\mathrm{d}^2\psi_{n}(x)}{\mathrm{d}x^2} + V(x) = E\psi_{n}(x) \quad n = 2, 4, 6, \ldots, N \tag{7}$$

The Schrödinger's equations are solved as

$$\psi_{n-1}(x) = A_1 \mathrm{e}^{ik_{n-1}x} + B_1 \mathrm{e}^{-ik_{n-1}x} \quad \text{where} \quad k_{n-1} = \frac{\sqrt{2m(E)}}{\hbar} \quad n = 2, 4, 6, \ldots, N \tag{8}$$

$$\psi_n(x) = A_2 \mathrm{e}^{k_n x} + B_2 \mathrm{e}^{-k_n x} \quad \text{where} \quad k_n = \frac{\sqrt{2m(V-E)}}{\hbar} \quad n = 2, 4, 6, \ldots, N \tag{9}$$

The Schrödinger equations are written in the matrix of the equation as[24]

$$\begin{bmatrix} t_0 \mathrm{e}^{-ik_n} & -t_0 & 0 & 0 \\ -t_0 & \frac{\sin N \cdot k_{n-1}}{\sin(N-1)k_{n-1}} t_0 & -\frac{\sin k_{n-1}}{\sin N \cdot k_{n-1}} t_0 & 0 \\ 0 & -\frac{\sin k_{n-1}}{\sin(N-1)k_{n-1}} t_0 & \frac{\sin N \cdot k_{n-1}}{\sin(N-1)k_{n-1}} t_0 & -t_0 \\ 0 & 0 & -t_0 & -t_0 \mathrm{e}^{-ik_n} \end{bmatrix} \times \begin{bmatrix} 1 \\ \psi_1 \\ \psi_N \\ 1 \end{bmatrix} = \begin{bmatrix} -t_0 \mathrm{e}^{ik_n} \\ t_0 \\ 0 \\ 0 \end{bmatrix} \tag{10}$$

where t_0 is the length of the potential barrier, $k_{n-1} = \frac{\sqrt{2m(E)}}{\hbar}$, $k_n = \frac{\sqrt{2m(V-E)}}{\hbar}$, m is the effective mass, E the energy bond, V the potential energy, N the number of dots and $\psi_{1,}\psi_n$ are Schrödinger's equations that were defined previously.

Therefore, the transmission coefficient of a homogeneous linear QD array SET is written as

$$T = \left[\frac{2\sin\sqrt{\frac{2mE}{\hbar^2}}\sin\sqrt{\frac{2(E-E_g)}{ta'''}}}{\mathrm{e}^{-i\sqrt{\frac{2mE}{\hbar^2}}} \cdot \sin(N+1)\sqrt{\frac{2(E-E_g)}{ta'''}} - 2\sin N \cdot \sqrt{\frac{2(E-E_g}{ta'''}} + \mathrm{e}^{i\sqrt{\frac{2mE}{\hbar^2}}} \cdot \sin(N+1)\sqrt{\frac{2(E-E_g)}{ta'''}}} \right] \tag{11}$$

where m is the effective mass, E the energy bond, E_g the band gap fullerene, $\hbar$ Plank's constant, $a''' = 3a_{c\text{–}c}$, $a_{c\text{–}c} = 1.42$ Å is cthe arbon–carbon bond length, $t = 2.7$ eV is the nearest-neighbor carbon–carbon tight-binding overlap energy and N is the number of QDs.

The dispersion relationship model is based on the wave number k as a function of the energy bond E as[25,26]

$$k = \left(\frac{2(E - E_g)}{ta'''} \right)^{\frac{1}{2}} \tag{12}$$

Therefore, the quantum drain current can be calculated by the Landauer formalism as[27,28]

$$I_d = \int_0^{\eta} F(E) \cdot T(E) \mathrm{d}E \tag{13}$$

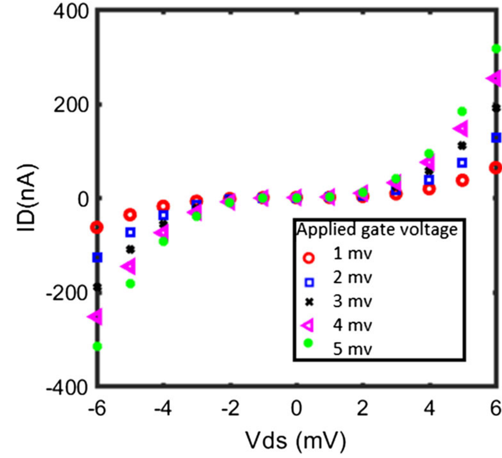

Fig. 7. I–V curves of a homogenous linear QD array fullerene SET for different applied gate voltages.

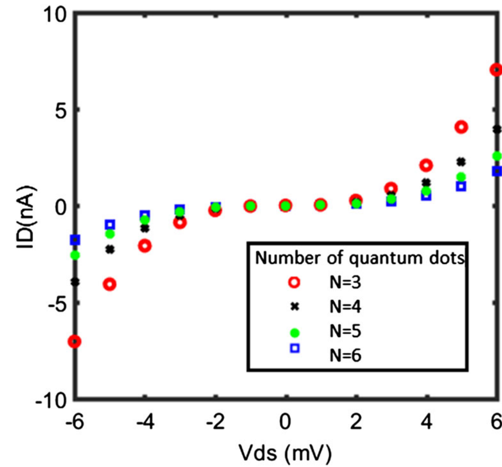

Fig. 8. I–V curves of a homogenous linear QD array fullerene SET for different numbers of QDs.

where $T(E)$ is the transmission coefficient of a homogenous linear fullerene QD array SET. Furthermore, $F(E)$ is a probability of distribution function as

$$f(E) = \left(\frac{1}{\exp\left(\frac{E-E_F}{k_B T}\right) + 1} \right) \tag{14}$$

Finally, a model is suggested for the drain current of a homogenous linear fullerene QD array SET in the parabolic region, which is calculated by

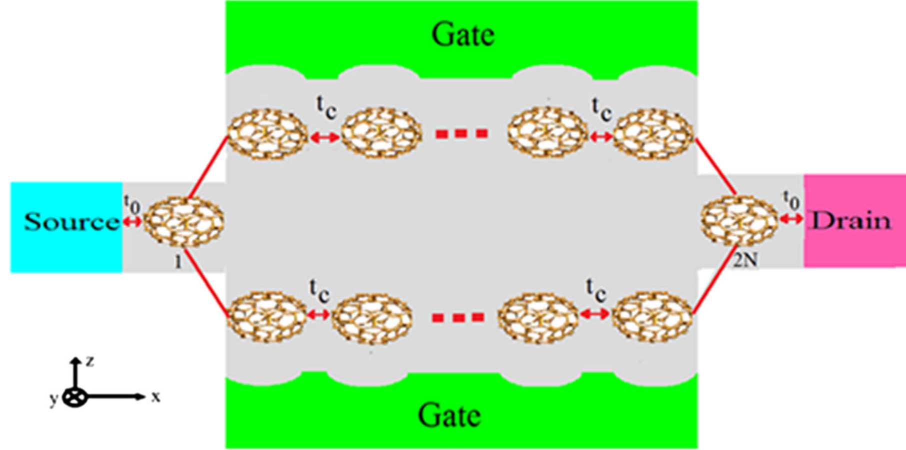

Fig. 9. The structure of a SET with homogeneous ring QD arrays.

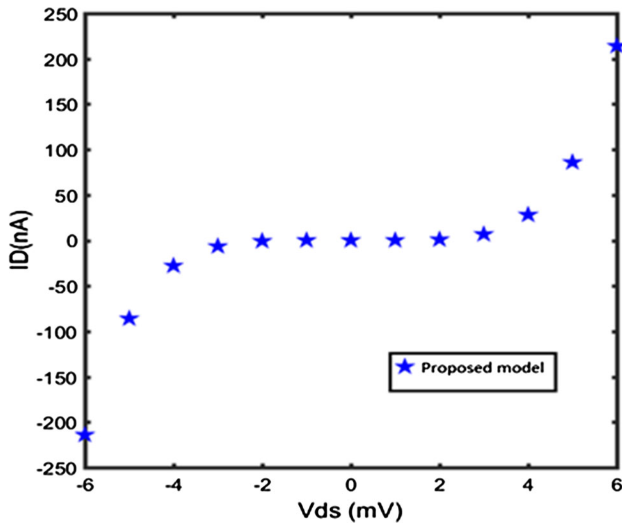

Fig. 10. I–V curve of a homogenous ring QD array fullerene SET at room temperature.

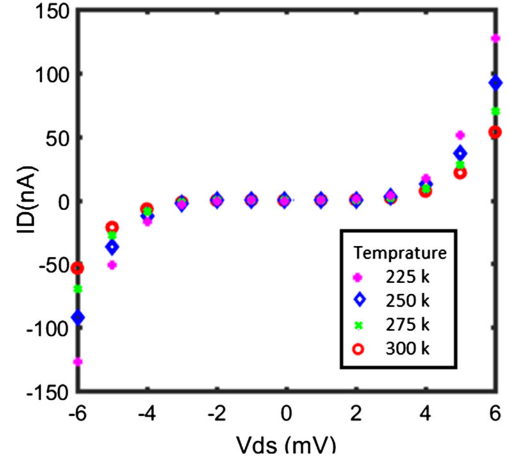

Fig. 11. I–V curves of a homogenous ring QD array fullerene SET at different temperatures.

$$I_d=\int_0^{\eta}\left[\frac{(c_2^2x^2L^2-6)\left[c_2xL\sqrt{c_1(x+d)}^3-6c_2xL\sqrt{c_1(x+d)}\right]xK_BT\cdot dx}{e^{-ic_2xL}\left[6(N+1)L\sqrt{c_1(x+d)}-\left[(N+1)L\sqrt{c_1(x+d)}\right]^3\right]-2\left[6NL\sqrt{c_1(x+d)}-\left[NL\sqrt{c_1(x+d)}\right]^3\right]+e^{ic_2x}\left[6(N-1)L\sqrt{c_1(x+d)}-\left[(N-1)L\sqrt{c_1(x+d)}\right]^3\right]}\right]^2\cdot\frac{1}{e^{x-\eta}+1} \quad (15)$$

where L is the island length, $c_1=\left(\frac{2mK_BT}{\hbar}\right)$, $c_2=\left(\frac{32mK_BT}{9\hbar(t\cdot a_{c-c})^2}\right)$, $d=\frac{E_g}{K_B\cdot T}$, $x=\frac{E-E_g}{K_BT}$, $\eta=\frac{E_F-E_g}{K_BT}$, T is the temperature, K_B the Boltzmann constant, N the number of dots, m the effective mass, $\hbar$ Plank's constant, a_{c-c} = 1.42 Å is carbon–carbon bond length, t = 2.7 eV is the nearest-neighbor carbon–carbon tight-binding overlap energy, E is the energy bond, E_g band gap of fullerene and E_F is the Fermi energy.

The curve of current versus voltage based on the proposed model as a homogenous linear QD array fullerene SET is plotted in Fig. 5.

The effects of some factors such as temperature, applied gate voltage and the number of QDs have been investigated. The current versus voltage

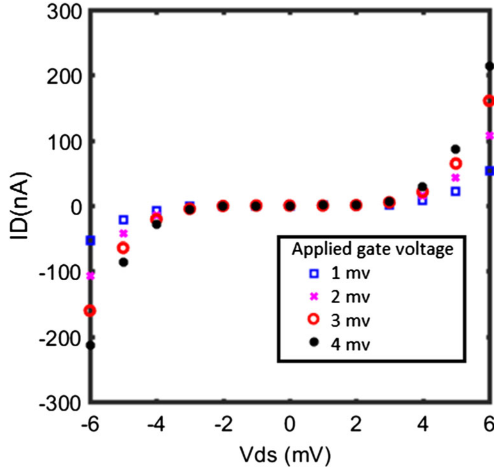

Fig. 12. I–V curves of a homogenous ring QD array fullerene SET for different gate voltages.

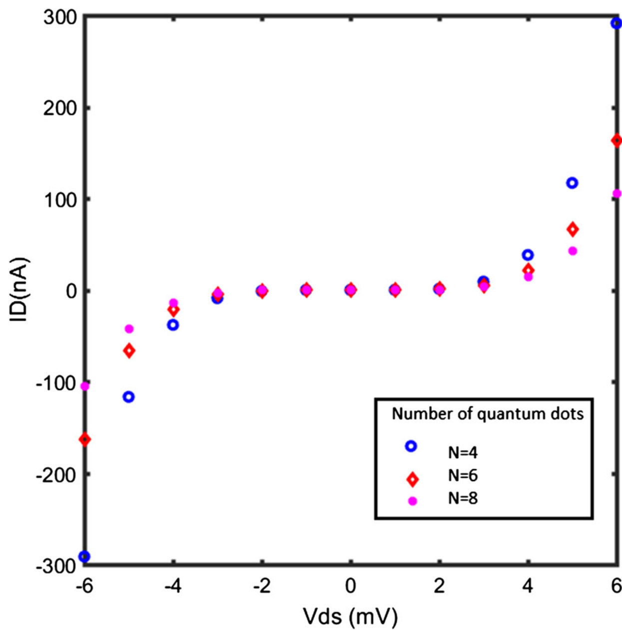

Fig. 13. I–V characteristics of a homogenous ring QD array fullerene SET with different numbers of QDs.

characteristics of the proposed model at different temperatures are plotted in Fig. 6.

The result of the temperature up to room temperature shows that the CB and the threshold voltage increase at higher temperature. The second factor is the applied gate voltage and its effect on the CB is reported in Fig. 7.

The variations in Fig. 7 show that increasing the applied gate voltage decreases the CB and threshold voltage. Another effective factor is the number of QDs and their effect is shown in Fig. 8.

The difference between the curves in Fig. 8 demonstrate that the number of QDs has a direct effect on the current. Moreover, the second state as

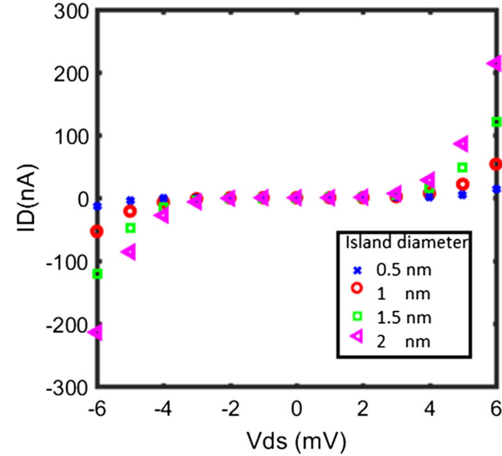

Fig. 14. I–V curves of a homogenous ring QD array fullerene SET for different island diameters.

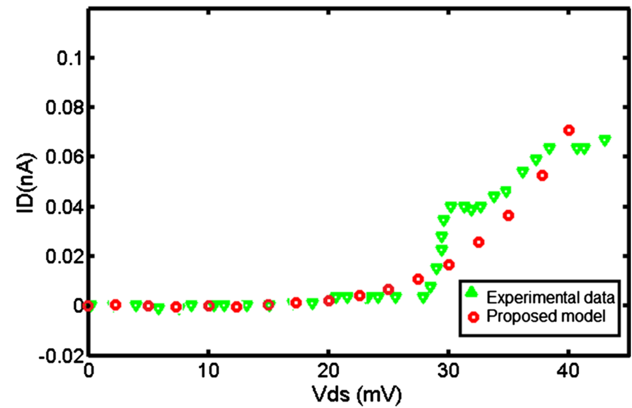

Fig. 15. The comparison of current versus voltage curves based on the proposed model of a fullerene SET and experimental data.

a homogeneous ring structure consists of 2 N QDs in two symmetrical rows has been investigated. Its structure is shown in Fig. 9. Each of QDs is assumed a quantum well in Schrödinger's equations. These equations are solved, so the solution is written as a matrix[24]

$$\begin{bmatrix} t_0 e^{-ik_n} & -t_0 & 0 & 0 \\ -t_0 & \frac{2\sin k_{n-1}\cdot\sin N\cdot k_{n-1}}{\sin N k_{n-1}} t_0 & -\frac{2\sin k_{n-1}}{\sin N\cdot k_{n-1}} t_0 & 0 \\ 0 & -\frac{2\sin k_{n-1}}{\sin N k_{n-1}} t_0 & \frac{\sin k_{n-1}\cos N\cdot k_{n-1}}{\sin N k_{n-1}} t_0 & -t_0 \\ 0 & 0 & -t_0 & -t_0 e^{-ik_n} \end{bmatrix} \begin{bmatrix} 1 \\ \psi_1 \\ \psi_{2N} \\ 1 \end{bmatrix} = \begin{bmatrix} -t_0 e^{ik_n} \\ t_0 \\ 0 \\ 0 \end{bmatrix} \tag{16}$$

where t_0 is the length of the potential barrier, $k_{n-1} = \frac{\sqrt{2m(E)}}{\hbar}$, $k_n = \frac{\sqrt{2m(V-E)}}{\hbar}$, m is the effective mass, E the energy bond, V the potential energy, N the the number of dots and ψ_1, ψ_{2n} are Schrödinger's equations as

$$\psi_{n-1}(x) = A_1 e^{ik_{n-1}x} + B_1 e^{-ik_{n-1}x} \quad \text{where} \quad k_{n-1} = \frac{\sqrt{2m(E)}}{\hbar} \quad n = 2, 4, 6, \ldots, N \tag{17}$$

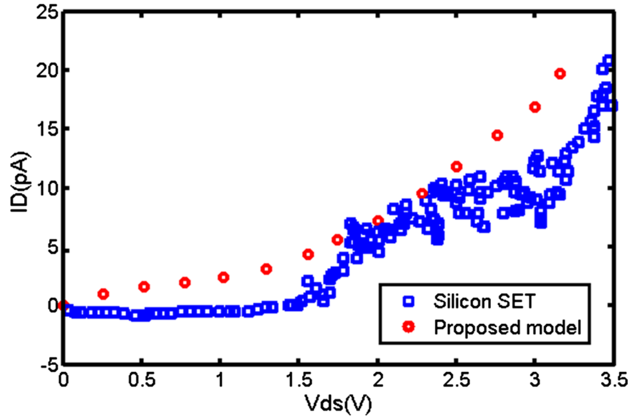

Fig. 16. Drain current versus voltage characteristics of QD array SETs. The red circles shows the current of the QD array fullerene SET at room temperature, and the blue squares show experimental data of the QD array silicon SET at room temperature (Color figure online).

$$\psi_{2n} = A_2 e^{k_n x} + B_2 e^{-k_n x} \quad \text{where} \quad k_n = \frac{\sqrt{2m(V-E)}}{\hbar} \quad n = 2, 4, 6, \ldots, N \tag{18}$$

Therefore, the transmission coefficient of a homogeneous ring QD array SET is given by

$$T = \left[\frac{4\sin\sqrt{\frac{2mE}{\hbar^2}}\sin\sqrt{\frac{2(E-E_g)}{ta'''}}\sin N\sqrt{\frac{2(E-E_g)}{ta'''}}}{\left(2\sin\sqrt{\frac{2(E-E_g)}{ta'''}}\cos N\sqrt{\frac{2(E-E_g)}{ta'''}} - e^{i\sqrt{\frac{2mE}{\hbar^2}}}\sin N.\sqrt{\frac{2(E-E_g)}{ta'''}}\right)^2 - 4\sin^2\sqrt{\frac{2(E-E_g)}{ta'''}}}\right] \tag{19}$$

where m is the effective mass, E the energy bond, E_g the band gap fullerene, $\hbar$ Plank's constant, $a''' = 3a_{c-c}$, $a_{c-c} = 1.42$ Å is cthe arbon–carbon bond length, $t = 2.7$ eV the nearest-neighbor carbon–carbon tight-binding overlap energy and N is the number of QDs.

The drain current of a homogeneous ring QD array SET is modeled by

$$I_d = \int_0^\eta \left[\frac{\dfrac{0.22(6c_2xL - c_2^3x^3L^3)\left[6\sqrt{c_1(x+d)}L - \sqrt{c_1(x+d)}^3L^3\right]\left[6NL\sqrt{c_1(x+d)} - N^3L^3\sqrt{c_1(x+d)}^3\right]xK_BT\cdot dx}{\left(2\left[6L\sqrt{c_1(x+d)} - L^3\sqrt{c_1(x+d)}^3\right]\cdot\left[2-\left[NL\sqrt{c_1(x+d)}\right]^2\right]\right.}}{\left.+e^{ic_2xL}\left[12NL\sqrt{c_1(x+d)} - \left[2N^3L^3\sqrt{c_1(x+d)}^3\right]\right]\right)^2 - 4\left[12L\sqrt{c_1(x+d)} - 2L^3\sqrt{c_1(x+d)}^3\right]^2}\right]^2 \cdot \frac{1}{e^{x-\eta}+1} \tag{20}$$

where L is the island length, $C_1 = \left(\frac{2m\cdot K_B\cdot T}{\hbar}\right)$, $C_2 = \left(\frac{32\cdot m\cdot K_B\cdot T}{9\hbar(t\cdot a_{c-c})^2}\right)$, $d = \frac{E_g}{K_B\cdot T}$, $x = \frac{E-E_g}{K_BT}$, $\eta = \frac{E_F-E_g}{K_BT}$, T is the temperature, K_B the Boltzmann constant, N the number of dots, m the effective mass, $\hbar$ Plank's constant, $a_{c-c} = 1.42$ Å is cthe arbon–carbon bond length, $t = 2.7$ eV the nearest-neighbor carbon–carbon tight-binding overlap energy, E the energy bond, E_g the band gap of fullerene and E_F the Fermi energy.

The characteristic of current versus voltage based on the proposed model of a ring QD array fullerene SET is reported in Fig. 10.

The effective factors such as temperature, gate voltage, the number of QDs and island diameter have been investigated. The effect of temperature is reported in Fig. 11.

The changes of I–V curves in Fig. 11 are the direct effect of temperature on the CB and the threshold voltage. Furthermore, the effect of applied gate voltage is investigated in Fig. 12.

The curves of Fig. 12 show that increasing applied gate voltages decrease the CB and the threshold voltage. Moreover, the effect of the number of QDs on the I–V curve is reported in Fig. 13.

Curves in Fig. 13 confirm that increasing the number of QDs increases the CB and threshold voltage. Furthermore, the effect of island diameter is investigated in Fig. 14.

The curves of Fig. 14 show that increasing the island diameter decreases the CB and the threshold voltage.

The comparison study indicates that a homogenous linear QD array fullerene SET has a lower CB and zero current range than a homogenous ring QD array fullerene SET. Furthermore, the drain

current versus voltage characteristics of the proposed model and experimental data of a fullerene SET extracted from the literature are shown in Fig. 15.[16]

The comparison study of the proposed model and experimental data confirms the good agreement between them. Moreover, the model of the QD array fullerene SET is compared with the QD array silicon SET at room temperature extracted from the literature in Fig. 16.[29]

The analysis of the I–V curve in Fig. 16 shows that the CB range is observed between the drain bias of 0 V and 1.5 V, and therefore the threshold voltage is 1.5 V in the QD array silicon SET, but the CB is in the millivolt range and also it is much smaller in the QD array fullerene SET than in the silicon one. Moreover, the result of the comparison study confirms that the QD array fullerene SET has a better operation at room temperature, and therefore has more reliability. Hence, this result demonstrates that a silicon dot can be replaced by a fullerene dot in a QD array SET.

CONCLUSION

SETs as nanoscale devices with low power consumption play important roles in the nanotechnology era because their operation depends on transferring an electron between tunnel junctions. SETs work at cryogenic temperature which has been reported as an operation limitation for these devices. QD arrays can reduce this temperature limitation but they increase the threshold voltage. In this research, the SETs with fullerene QD arrays in two states, linear and ring, have been investigated and their characteristics of current versus voltage have been modeled. a comparison study was carried out which indicates that the threshold voltage of a QD array Fullerene SET is lower than a QD array silicon SET. Furthermore, a linear QD array SET has a lower Coulomb blockade range and more reliability than a ring QD array SET. Moreover, the applied gate voltage and QD diameters have direct effects on its current. The SETs with different numbers of QDs were investigated, while a comparison study of their I–V curves shows that the number of QDs directly affect the CB range. The results predict that a QD array silicon SET can be replaced by a linear QD array fullerene SET in future nanotechnology.

REFERENCES

1. G.E. Moore, *Proc. IEEE* 38, 114 (1965).
2. J.D. Meindl, *Micropower Circuits* (New York: Wiley, 1969).
3. D. Flynn, R. Aitken, A. Gibbons, and K. Shi, *Low Power Methodology Manual*, 1st ed. (New York: Springer, 2007).
4. C. Piguet, *Low-Power CMOS Circuits: Technology, Logic Design and CAD Tools* (London: Taylor and Francis, 2006).
5. V.V. Shorokhov, D.E. Presnov, S.V. Amitonov, Y.A. Pashkin, and V.A. Krupenin, *Nanoscale* 9, 613 (2017).
6. F. Wang, J. Fang, Sh. Chang, S. Qin, X. Zhang, and H. Xu, *Phys. Lett. A* 381, 476 (2017).
7. V. Khadem Hosseini, M.T. Ahmadi, S. Afrang, and R. Ismail, *J. Electron. Mater.* 46, 4294 (2017).
8. H. Zheng, M. Asbahi, S. Mukherjee, C.J. Mathai, K. Gangopadhyay, J.K.W. Yang, and Sh. Gangopadhyay, *Nanotechnology* 26, 35 (2015).
9. F. Willy and Y. Darma, *J. Phys. Conf. Ser.* 739, 012048 (2016).
10. W.A. Schoonveld, J. Wildeman, D. Fichou, P.A. Bobbert, B.J. van Wees, and T.M. lapwijk, *Nature* 404, 998 (2000).
11. J. Park, A.N. Pasupathy, J.I. Goldsmith, C. Chang, Y. Yaish, J.R. Petta, M. Rinkoski, J.P. Sethna, H.D. Abruña, P.L. McEuen, and D.C. Ralph, *Nature* 417, 722 (2002).
12. M. Ejrnaes, M.T. Savolainen, M. Manscher, and J. Mygind, *Phys. C: Superconduct.* 372, 1353 (2002).
13. K. Lee, G. Kulkarni, and Z. Zhong, *Nanoscale* 8, 7755 (2016).
14. A.S. Cordan, A. Goltzene, Y. Herve, M. Mejias, C. Vieu, and H. Launois, *J. Appl. Phys.* 84, 3756 (1998).
15. A.S. Cordan, Y. Leroy, A. Goltzené, A. Pépin, C. Vieu, M. Mejias, and H. Launois, *J. Appl. Phys.* 87, 345 (1998).
16. H. Park, J. Park, A.K.L. Lim, E.H. Anderson, A.P. Alivisatos, and P.L. McEuen, *Nature* 407, 57 (2000).
17. J.R. Tucker, *J. Appl. Phys.* 72, 4399 (1992).
18. D. Averin and K. Likharev, *Mesoscopic Phenomena in Solids*, 1st ed. (Amsterdam: North-Holland, 1991), p. 173.
19. L. Sheela, N.B. Balamurugan, S. Sudha, and J. Jasmine, *J. Electr. Eng. Technol.* 9, 1670 (2014).
20. K.K. Likharev, *Proc. IEEE* 87, 606 (1999).
21. M. Amman, R. Wilkins, E. Ben-Jacob, P.D. Maker, and R.C. Jaklevic, *Phys. Rev. B* 43, 1146 (1991).
22. M.G. Reuter, T. Seideman, and M.A. Ratner, *Nano Lett.* 11, 4693 (2011).
23. K. Peng Dou and C. Cheng Kaun, *J. Phys. Chem. C* 120, 18939 (2016).
24. H. Christian, C.H. Schiegg, M. Dzierzawa, and U. Eckern, *J. Phys. Condens. Matter* 29, 055301 (2017).
25. G.W. Semenoff, *Phys. Rev. Lett.* 53, 2449 (1984).
26. P. Wallace, *Phys. Rev.* 71, 622 (1947).
27. R. Landauer, *Phil. Mag.* 21, 863 (1970).
28. S. Datta, *Electronic Transport in Mesoscopic Systems*, 2nd ed. (Cambridge: Cambridge University Press, 2012).
29. A.Z. Khan Durrani, *Single-Electron Devices and Circuits in Silicon* (London: Imperial College Press, 2010), p. 127.